

Evaluation of Quantum Approximate Optimization Algorithm based on the approximation ratio of single samples

Jason Larkin*, Matías Jonsson*†, Daniel Justice*, and Gian Giacomo Guerreschi‡

*Software Engineering Institute, Carnegie Mellon University, Pittsburgh, Pennsylvania 15213

†Department of Physics, Carnegie Mellon University, Pittsburgh, Pennsylvania, 15213

‡Intel Labs, Santa Clara, California 95054

Abstract—The Quantum Approximate Optimization Algorithm (QAOA) is a hybrid quantum-classical algorithm to solve binary-variable optimization problems. Due to its expected robustness to systematic errors and the short circuit depth, it is one of the promising candidates likely to run on near-term quantum devices. We project the performance of QAOA applied to the Max-Cut problem and compare it with some of the best classical alternatives, both for exact or approximate solution. When comparing approximate solvers, their performance is characterized by the computational time taken to achieve a given quality of solution. Since QAOA is based on sampling, we introduce performance metrics based on the probability of observing a sample above a certain quality. In addition, we show that the QAOA performance varies significantly with the graph type. By selecting a suitable optimizer for the variational parameters and reducing the number of function evaluations, QAOA performance improves by up to 2 orders of magnitude compared to previous estimates. Especially for 3-regular random graphs, this setting decreases the performance gap with classical alternatives.

I. INTRODUCTION

The challenge for near-term noisy intermediate scale quantum computing (NISQ) is to demonstrate quantum advantage, where some computation is performed by a quantum computer that is classically computationally intractable [1]. While “quantum supremacy” may have been demonstrated for the task of sampling the outcome of random quantum circuits [2]–[6], practical applications of post-classical computation still need to be demonstrated.

A common practical problem used as a benchmark for both high performance classical and quantum computing is Max-Cut, a graph partition problem with applications in domains such as machine scheduling,[7] image recognition,[8] electronic circuit layout [9], and software verification/validation [10], [11]. Max-Cut is a NP-hard problem[12] and is naturally phrased as a Quadratic Unconstrained Binary Optimization (QUBO) problem.

Here, we investigate the Quantum Approximate Optimization Algorithm (QAOA) [13] applied to Max-Cut

for different types of graphs. QAOA is a hybrid quantum-classical algorithm based on a circuit whose variational parameters are optimized with respect to the specific instance to solve. It is formulated as a heuristic approach with the goal of approximating the solution of hard problems. We numerically simulate the execution of QAOA experiments and estimate the time required by noiseless hardware to provide candidate solutions above a certain approximation ratio. For instances of small size and reasonable convergence criteria, QAOA often returns the global solution.

We compare QAOA against a list of the best performing classical solvers[14], [15] in terms of time-to-solution[16], [17] and quality for a range of graph types [18]–[21]. One of the main contributions of this work is the definition of the framework for such comparison. From its original formulation, QAOA is expected to return the best candidate solution found in the course of the optimization. However, the objective that guides such optimization is an expectation value averaged over multiple candidate solutions. Until now, most studies relied on concentration arguments to report the average value instead of the best single outcome [22]–[26]. In this work, given a desired approximation ratio, we formulate the performance of QAOA as the time needed before at least one sample with approximation ratio above the desired threshold is observed with probability at least 50%.

This paper is organized as follows: Section II describes QAOA, its applications and some previous results. Section III introduces the framework to report QAOA performance based on the approximation ratio of single samples. It also provides information about how we perform the numerical simulations and the classes of graphs we consider. The results from the numerical simulations are compared with classical solvers in Section IV, and the results are discussed in Sections V and VI.

II. QUANTUM APPROXIMATE OPTIMIZATION ALGORITHM

The Quantum Approximate Optimization Algorithm (QAOA) is a hybrid quantum-classical algorithm that variationally improves shallow quantum circuits to prepare states with desired properties. In its original formulation, the target state corresponds to the solution of binary-variable minimization problems [13]. The cost function is represented by a linear combination of operators that are diagonal in the Z basis:

$$\hat{C} = \sum_{m=1}^M \hat{C}_m, \quad (1)$$

where M is the number of terms, each proportional to the product of a few Z Pauli matrices. The observable \hat{C} is obtained from the classical cost function by substituting classical binary variables $z_k \in \{-1, +1\}$ with quantum operators \hat{Z}_k , the Z Pauli matrix on qubit k . For Quadratic Unconstrained Binary Optimization (QUBO) problems, each term \hat{C}_m is proportional to $\hat{Z}_i \hat{Z}_j$ for a certain pair (i, j) of qubits.

The QAOA circuit is obtained by alternating two blocks of quantum operations for a total of p times each, with p being an adjustable parameter. Each block is characterized by a scalar parameter (denoted either by γ_k or β_k) and their values uniquely determine the output state. We denote the variational state prepared by the QAOA circuit as:

$$|\gamma, \beta\rangle = e^{-i\beta_p \hat{B}} e^{-i\gamma_p \hat{C}} \dots e^{-i\beta_1 \hat{B}} e^{-i\gamma_1 \hat{C}} |+\rangle^{\otimes N}, \quad (2)$$

where $B = \sum_k \hat{X}_k$ is the sum of the X Pauli matrices associated to each qubit, $|+\rangle = (|0\rangle + |1\rangle)/\sqrt{2}$, and N is the number of qubits. The circuit's depth is linear in p and the number of its parameters is $2p$. In this work, $(\gamma, \beta) = (\gamma_p, \beta_p, \dots, \gamma_2, \beta_2, \gamma_1, \beta_1)$

QAOA has already been applied to a growing number of combinatorial optimization problems like community detection [23], vertex cover [27], maximum independent set [28], and tail assignment [29]. However its most studied application is probably to a graph partition problem called Max-Cut. Its formulation is easily stated: divide the vertices of a graph in two groups and count the number of edges connecting vertices of different groups. These edges are usually said to be “cut” by the partition. The answer to the problem is returning the partition with the largest number of cut edges. Despite its simplicity, Max-Cut appears in many domains.[7]–[11]

To formulate Max-Cut as a binary variable problem, assign to each vertex a label from $\{+1, -1\}$ indicating to which of the two groups it belongs. Since QAOA is a minimization problem, we use as cost function the (additive) inverse of the number of cut edges. The

quantum version of such a cost function can be expressed as a QUBO formula plus a constant term:

$$\hat{C} = -\frac{M}{2} + \frac{1}{2} \sum_{(i,j) \in E} \hat{Z}_i \hat{Z}_j, \quad (3)$$

where E is the set of edges of the graph to partition and M its number of edges.

III. METHODS

A central quantity in the optimization of QAOA circuits is the expectation value of the cost function observable \hat{C} on state $|\gamma, \beta\rangle$ in Eq. (2):

$$F_p(\gamma, \beta) = \langle \gamma, \beta | \hat{C} | \gamma, \beta \rangle. \quad (4)$$

The minimization of F_p is a good proxy for the desired goal of preparing the ground state of \hat{C} . In fact, the ground state is the solution of:

$$\min_{|\psi\rangle} \langle \psi | \hat{C} | \psi \rangle \quad (5)$$

and it is reasonable to expect that, for expressive enough QAOA circuits, state $|\gamma, \beta\rangle$ can achieve large overlap with the ground state by minimizing F_p with respect to (γ, β) .

In practical implementations of QAOA there are two subtle points related to the choice of $F_p(\gamma, \beta)$ as the function to minimize. First, one does not experimentally access an observable's expectation value directly, but can only estimate it by obtaining many assignments of the problem's variables and averaging their cost function values. This procedure is very natural since \hat{C} is diagonal in the computational basis and the assignments are obtained by measuring all qubits in the Z basis. Second, while F_p is the objective function of the minimization, the result reported at the end of QAOA experiments is the minimum cost function value among all the observed samples and not their average.

A. Sampling of Approximation Ratios

To clarify the above remarks, we introduce the “cost distribution” associated to $|\gamma, \beta\rangle$. The QAOA state of N qubits can be represented in the Z basis as:

$$|\gamma, \beta\rangle = \sum_{z \in \{-1, +1\}^N} \alpha_z |z\rangle \langle z| \quad (6)$$

where $z = (z_1, z_2, \dots, z_N)$ and $|z\rangle$ is the unique common eigenstate of every \hat{Z}_k with eigenvalue z_k . Since the cost function is diagonal in the Z basis, one has:

$$\hat{C} |z\rangle = C(z) |z\rangle. \quad (7)$$

The cost distribution of $|\gamma, \beta\rangle$ is the probability distribution $P_{\text{Cost}}^{(\gamma, \beta)}$ that associates to each cost function value c the probability:

$$P_{\text{Cost}}^{(\gamma, \beta)}(c) = \sum_{z \text{ s.t. } C(z)=c} |\alpha_z|^2. \quad (8)$$

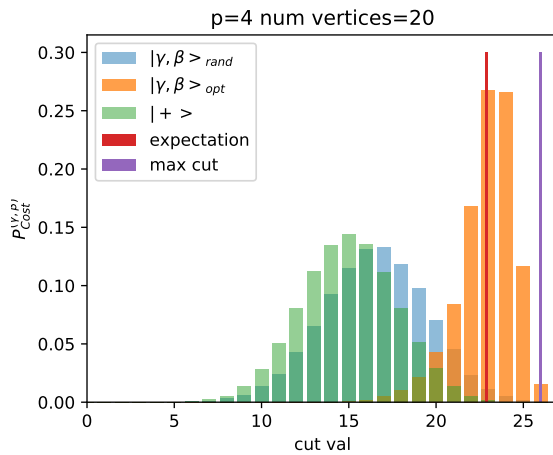


Figure 1: Cut distributions for Max-Cut on a random 3-regular graphs with 20 vertices. Three distributions are plotted, each characterized by different values of the parameters (γ, β) . In green, the case of $\gamma_k = \beta_k = 0$ for each $k = 0, 1, \dots, p$ corresponding to the case in which every graph partition has the same probability $1/2^N$. In blue, the distribution for a random choice of parameters, and in orange the one at the end of the optimization process. The vertical red line indicates the expectation value of the orange distribution. The maximum cut value is indicated by the purple column.

When clear from the context, superscript (γ, β) will be omitted. In the specific case of Max-Cut, we sometimes use the term “cut distribution” to indicate the same concept but w.r.t. the cut value. Since the cut value is the additive inverse of the cost value, one has $P_{\text{Cut}}(c) = P_{\text{Cost}}(-c)$.

Note that for Max-Cut the probability distribution P_{Cut} can be fully described by an exponentially smaller number of values than the 2^N amplitudes necessary to describe $|\gamma, \beta\rangle$. In fact, there are at most $\mathcal{O}(N^2)$ edges in any graph with N vertices, and therefore only the same number of distinct values of $C(z)$. This allows for an effective visualization of the result of optimizing the QAOA circuit. Fig. 1 shows the cut distribution when each partition is equally probable (corresponding to a QAOA circuit with $\gamma_k = \beta_k = 0$ for each $k = 0, 1, \dots, p$), and compare it to the cost distribution for a random choice of parameters (here $p = 4$) and for optimized values of (γ, β) .

The cut distribution is strictly connected to the result of QAOA experiments. In fact, for a given (γ, β) , a single experimental run of the QAOA circuit returns a specific graph partition whose cut value is distributed according to $P_{\text{Cut}}^{(\gamma, \beta)}$. By repeating the experiment S times and collecting the corresponding cut values, one can

estimate $F_p(\gamma, \beta)$ as their average. Denoting with $z^{(s)}$ the partition observed in the s -th run, one has:

$$F_p(\gamma, \beta) = \lim_{S \rightarrow \infty} \sum_{s=1}^S C(z^{(s)}). \quad (9)$$

In practice, the estimate involves a finite number S of repetitions and past experiments used $S \sim 1000 - 10,000$ [26], [30]–[32].

Finally, it is important to remember that QAOA is an approximate algorithm which is not guaranteed to return the global solution, but aims at a good approximation. The quality of the solution is expressed in terms of the approximation ratio given by $F_p(\gamma, \beta')/c^*$, where (γ, β') indicates the parameters at the end of the optimization and $C^* = \min_z C(z)$ is the global minimum of the cost function. However, we highlight that the result of QAOA experiments for Max-Cut should be the largest cut value among all the observed samples and not its average over $P_{\text{Cut}}^{(\gamma, \beta')}$.

For this reason, we structure our analysis of the QAOA performance in terms of the number of circuit repetitions before a cut value above a certain approximation ratio is observed. Formally, consider the approximation ratio r and ask what is the probability of observing at least one cut value above $r|c^*|$ among the first K samples. When such probability exceeds 50%, meaning that the event is more probable than not, we return K as the expected number of repetitions to reach the desired approximation.

Denoting with $Q_{\text{Cut}}^{(\gamma, \beta)}$ the cumulative distribution of $P_{\text{Cut}}^{(\gamma, \beta)}$, the probability of observing at least one cut value with approximation ratio at least r while keeping the QAOA parameter unchanged is:

$$P_r(K) = 1 - \left[Q_{\text{Cut}}^{(\gamma, \beta)}(r|c^*|) \right]^K \quad (10)$$

since $Q_{\text{Cut}}^{(\gamma, \beta)}(r|c^*|)$ represents the probability of *not* observing a cut value above approximation ratio r . The expression can be easily adapted to the case of varying (γ, β) by considering the actual $Q_{\text{Cut}}^{(\gamma, \beta)}$ for each of the K samples. In our approach, we vary (γ, β) every S samples (the same parameter as in the finite version of the right hand side of Eq. (9)).

B. Quantum Simulation and Circuit Execution Time

All numerical simulations have been implemented using the Python interface of Intel Quantum Simulator (IQS) [33]. The simulator has been developed in C language for high-performance-computing environments and is released open-source [34]. It stores the state of N qubits as a vector with 2^N complex amplitudes that is updated to reflect the execution of quantum operations. The release includes special functionalities to facilitate the emulation of QAOA circuits: instead of decomposing

$e^{-i\gamma\hat{C}}$ into one- and two-qubit gates and simulating each of them sequentially, IQS performs a single update that reflects the global operation. In addition, it gives access to the probability distribution of the cut values, namely $P_{\text{Cut}}^{(\gamma,\beta)}$ introduced in the previous subsection.

In this numerical study, we have not considered the effect of incoherent errors and environmental noise. The decision was motivated by the substantial overhead required to describe the noise effects, overhead estimated to be a factor $\sim 1,000$. For the considerations of this work, the effect of noise affects the shape of $P_{\text{Cut}}^{(\gamma,\beta)}$ and we expect to deform it in two ways: increasing its spread and, for good values of the parameters (γ,β) , reducing its average cut-value. We leave this point to further investigations.

In the following analysis, we do not need to estimate the time to simulate QAOA circuits, but rather the time to execute them on actual hardware. In addition, we are not interested in modelling a specific quantum processor, but only in providing an order of magnitude estimate. To this extent, we consider two abstract architectures characterized by the same gate set but different connectivity: all-to-all and bi-dimensional square grid. The gate set includes parametrized one-qubit and two-qubit rotations, like $\exp(-i\beta\hat{X}_k)$ and $\exp(-i\beta\hat{Z}_j\hat{Z}_k)$, and all gates have the same duration $T_{\text{gate}} = 10\text{ ns}$. We assume additional $T_{\text{spam}} = 1\text{ }\mu\text{s}$ for state preparation and measurement (spam). These values are reasonable in the context of emerging NISQ-era architectures, especially for superconducting transmon qubits [2]. No further limitations of gate parallelism are considered, apart from the requirement that every qubit can be involved in at most one gate at a time. For the circuit compilation and to satisfy the connectivity constraints, we adopt the scheduler based on dynamical pattern optimization described in reference [35].

The two architectures give different estimates of the execution time for a single QAOA circuit. For the full connectivity, given a graph instance with maximum vertex degree d , one has:

$$T_{\text{circuit}}^{(FC)} = T_{\text{spam}} + ((d+1)T_{\text{gate}} + T_{\text{gate}})p, \quad (11)$$

where we used the result that one needs at most $(d+1)$ colors to color the edges of a graph with vertex degree d [36] and therefore $(d+1)$ layers of two-qubit gates may be required to implement each $e^{-i\gamma_k\hat{C}}$, while a single layer suffices for each $e^{-i\beta_k\hat{B}}$. We do not consider extra time between circuit repetitions in addition to T_{spam} , not even when (γ,β) needs to be updated (once in S repetitions).

For the square grid connectivity, the scheduler returns the circuit depth l in terms of the number of layers of

parallel gates. Thus, the time to execute a single QAOA circuit is:

$$T_{\text{circuit}}^{(2D)} = T_{\text{spam}} + l p T_{\text{gate}}. \quad (12)$$

C. Optimization of Variational Parameters

The performance of QAOA depends critically on the choice of depth p and variational parameters (γ,β) . Due to its connection with adiabatic quantum optimization [37], QAOA is capable of finding the global minimum in the $p \rightarrow \infty$ limit [38], but its performance is still being explored for finite p . [19], [28], [39]–[41] Early results suggested that for $p = 1$ QAOA provides an approximation ratio for the problem MAX3Lin2 that is better than its classical counterparts. However the improvement has since been overtaken by a new classical method [38].

A number of strategies have been utilized in recent work to determine optimized variational parameters, including local optimization [24], gradient-based methods [42], multi-start optimization [43], reinforcement learning [44], [45], and analytical prediction [19], [46]. In this work, we utilize a combination of local and multi-start optimization, and discuss the results from each. We utilize the Asynchronously Parallel Optimization Solver for finding Multiple Minima (APOSMM) [47], which has been used successfully with QAOA and graph clustering [43]. For local optimization we use the derivative-free Bound Optimization By Quadratic Approximation (BOBYQA) [48]. For APOSMM, we vary the total number of evaluations of the cost function n_{fev} as discussed in Section IV.

To demonstrate the APOSMM optimization process, Figure 2 shows the path followed by the optimizer in the parameter landscape with $p = 1$. In this work, we consider graphs of three types:

random k -regular : each and every vertex has exactly k edges, chosen randomly;

Erdős-Renyi : each of the $N(N-1)$ edges has probability p_E of being present, with unbounded vertex degree

random weights : complete graph with weights chosen uniformly at random in $[0, 1]$ (see Appendix B for a note on random weight graphs).

Each type can give rise to a distinct graph class, for example by specifying the non-negative integer parameter k or the continuous parameter $p_E \in [0, 1]$.

For each graph type, the optimization landscape is distinct. For 3-regular graphs, the landscape is characterized by minima separated without plateaus. The variational parameters exhibit periodicity within the domain considered, which has been demonstrated previously [49], [50]. For Erdős and random weights, the landscape minima begin to concentrate and plateaus appear. These

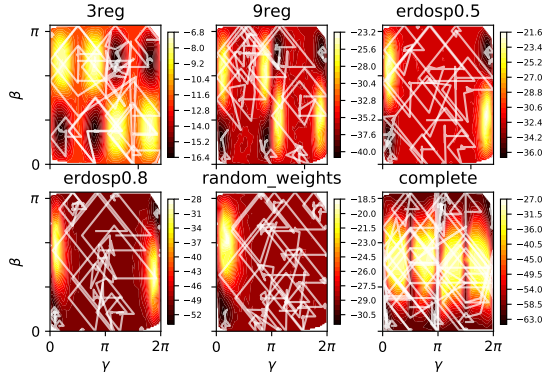


Figure 2: Optimization landscape (see Eq. (1)) for QAOA applied to the Max-Cut problem on graphs with $N = 16$ vertices. Several type of graphs are considered, from left to right and top to bottom: random 3-regular, random 9-regular, Erdős $p_E = 0.5$, Erdős $p_E = 0.8$, random weights, and the complete graph. As the graph structure changes and noticeably as the vertex degree increases, first from random 3- to 9-regular and then to Erdős and random weights, the global minimum becomes narrower and local plateaus appear.

plateaus create many local minima that are suboptimal and act as trap for the local optimization making it challenging for APOSMM to find the global minima (the path in parameter space is drawn as white traces). Similar difficulties in finding optimized parameters have been noted for QAOA and associated to the concentration of optimal parameters into a small region of the parameter space for random weight graphs [19].

Recently, it has been observed that good parameters obtained after the optimization of a specific instance, perform well also for other instances of the same class and even for different instance sizes. Analytical arguments [51] suggest that numerical observations [24], [52] may apply to a broad class of random graphs. We collect supporting evidence in Figure 3. There are two aspects worth observing: first, in any single plot the probability distribution has a structure connected to the concentration of optimized values of the parameters. Second, for each graph type, moving along the same row from left to right (*i.e.* increasing N), the distribution seems to converge suggesting that it may be preserved for $N > 20$. The latter observation is evident for random 3-regular graphs, but unclear for Erdős and random weight graphs.

In our case, Figure 3 is hardly conclusive. However, in the next Section we utilize the “trained” parameter sets optimized from small instance sizes to predict the performance for larger sizes. The effectiveness of this

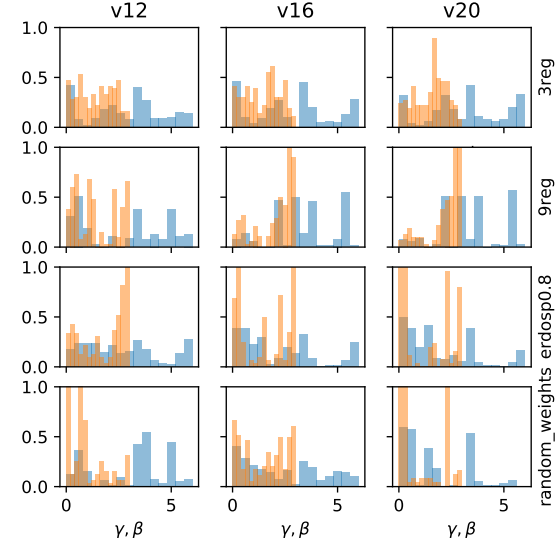


Figure 3: The distribution of variational parameters (γ, β) with $p = 4$ for different graph types and sizes. Every plot includes all parameters γ_k, β_k for $k \leq p$, represented by the blue and orange distributions respectively. Each row of plots corresponds to the same graph type, from top to bottom: 3-regular, 9-regular, Erdős with $p_E = 0.8$ and random weights. The number of vertices in each graph varies according to the column, increasing from left to right $N = 12, 16, 20$.

technique can be seen as a posteriori justification of this choice.

IV. RESULTS

We visualize the cut probability P_{Cut} for several graph types and three p values in Figure 4 (a). The green distribution corresponds to the $p = 0$ case, while the orange distribution to $p = 2, 4, 8$ —from left to right—and optimized parameters (γ, β) . Panel (b) of the same figure reports the cost of parameter optimization. The optimization budget of APOSMM is denoted by n_{fev} and varies from 10,000 to 25,000 function evaluations. Each function evaluation corresponds to an estimate of F_p with $S = 1,000$ samples, a number smaller than those used in QAOA experiments to date [26], [30], [32]. For 3- and 9-regular graphs, optimized variational parameters are found for $p = 4, 8$ yielding distributions which have large overlap with the maximum cut value (see also Figure 1). For Erdős and random weight graphs, the distributions have less overlap, and increasing p and n_{fev} does not lead to an increase in overlap.

This can be seen in Figure 4 (b), which shows the expected number of circuit’s repetitions before the prob-

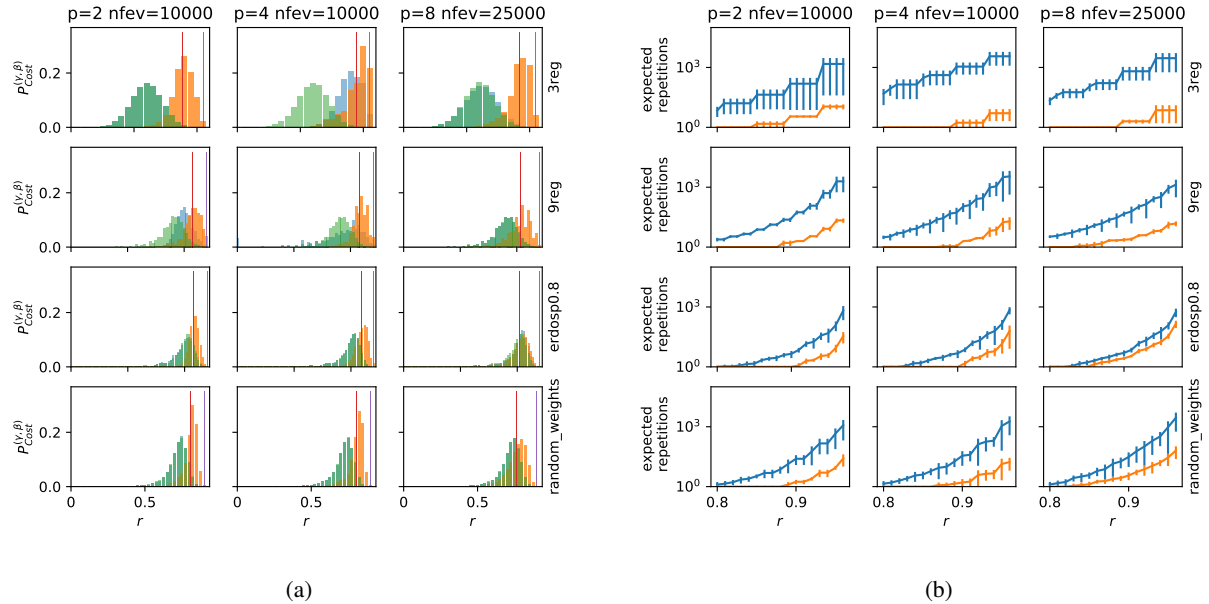


Figure 4: (a) Cut distributions for Max-Cut and several graph types, for a typical instance with $N = 16$ vertices (note the axes are scaled to approximation ratio r). From top to bottom: random 3-regular, random 9-regular, Erdős $p_E = 0.8$, and random weight graphs. In the first column, $p = 2$ and APOSMM is given a budget of $n_{\text{fev}} = 10,000$ function evaluations; second column $p = 4$ and $n_{\text{fev}} = 10,000$; third column $p = 8$ and $n_{\text{fev}} = 25,000$. Three distributions are plotted, each characterized by different values of the $2p$ parameters. In green, the case of $\gamma_k = \beta_k = 0$ for each $k = 1, 2, \dots, p$ corresponding to the case in which every graph partition has the same probability $1/2^N$. In blue, the distribution at an intermediate stage of the optimization and in orange the distribution for the optimized parameters. (b) Expected number of repetitions of the QAOA circuit required to observe at least one samples with given approximation ratio r . The blue line is obtained updating P_{Cut} every $S = 1,000$ samples during the optimization process. The orange line corresponds to sampling directly from the optimized distribution. We report the average over 10 instances and the vertical bars represent one standard deviation. Subplots are organized in rows and columns according to panel (a).

ability of observing a cut value with a given approximation ratio is at least 50% (see equation Eq. (10)). The blue line corresponds to the case in which the parameters are randomly initialized and then updated during the optimization. The orange line represents the case in which the optimized parameters are known from the start. It is not surprising that this knowledge reduces the QAOA cost by several orders of magnitude. The results in this panel are averaged over 10 random instances of each graph type, whereas panel (a) shows a typical instance.

For k -regular graphs and small instance size, shallow circuits corresponding to $p \leq 8$ are expressive enough for state $|\gamma, \beta\rangle$ to exhibit a large overlap with the ground state of \hat{C} . This is not the case for Erdős and random weights, resulting in over an order of magnitude larger expected number of circuit repetitions for a given approximation ratio. We project the implications of these results in the next figure by comparing the performance

with classical exact and approximate solvers.

We utilize the simple model for quantum processors described in Section III-B: noiseless devices with full and bi-dimensional square grid connectivity. The time to run a single QAOA circuit in the two architectures is given by Eq. (11) and Eq. (12) respectively. When multiplied by the number of circuit repetitions, we obtain the absolute-time performance of QAOA, here called WallTime. Figure 5 shows the WallTime of QAOA averaged over 10 random 3-regular graphs, for both quantum architectures and starting from random and optimized (γ, β) values. Also shown is the performance for a state-of-the-art exact solver (AKMAXSAT) [53] and a famous approximate algorithm (GW) [14]. We report the time to solution on the vertical axis, together with the quality of the approximate solution, expressed by its approximation ration r . It is clear that the exact solver provides a single datapoint located at $r = 1$, while the classical optimizer leads to a distribution of results.

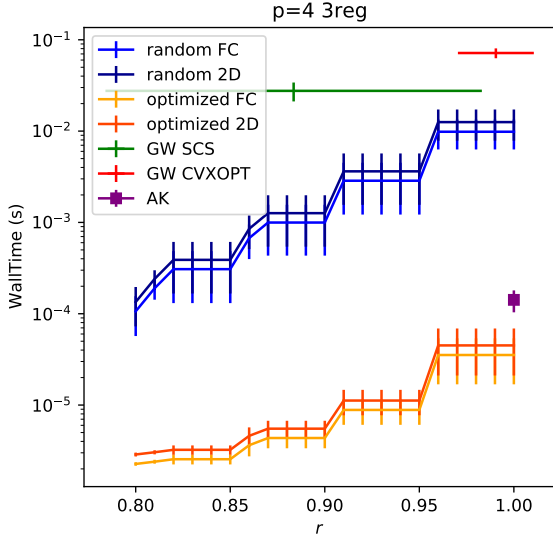


Figure 5: The WallTime performance for random 3-regular graphs with 16 vertices, averaged over 10 instances. The horizontal axis indicates the desired quality of the solution, expressed in terms of the approximation ratio r . The blue lines correspond to the performance of the local optimization attempts of the APOSMM training stage, with a large n_{fev} budget and initial random parameters. The label FC indicates results for a quantum processor with full connectivity and 2D with a square grid connectivity. The orange lines correspond to the performance using the optimized parameters found by training. For comparison, classical exact solvers (AK-MAXSAT) and approximate algorithms (GW) are also shown. Two semi-definite programming implementations (labelled SCS and CVXOPT from the name of their Python package) are used for GW. Vertical and horizontal (for GW) bars indicate one standard deviation of the instance average. More considerations in the main text.

In particular, we observe that the approximation ratio performance varies significantly for GW depending on which optimization method (CVXOPT or SCS) is used to solve its semi-definite relaxation. The performance of random and optimized QAOA varies by over 2 orders of magnitude, with optimized QAOA producing approximate and exact solutions competitively with both GW and AKMAXSAT.

We observe that the relative performance of GW compared to AKMAXSAT is surprising: an approximate solver is expected to be faster than an exact solver. Clearly this is not the case in our numerical study. There are multiple reasons for this situation and we

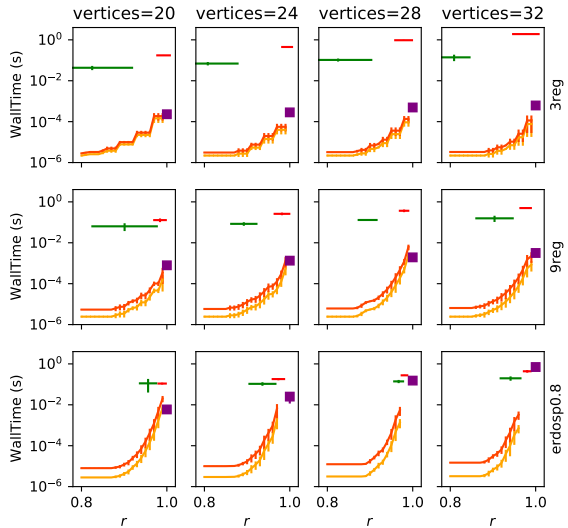


Figure 6: WallTime performance for QAOA, utilizing the trained parameters from the 16 vertex graphs (see Fig. 5), and compared against the classical exact (AKMAXSAT) and approximate (GW) solvers. For all graph types, QAOA is able to produce approximate solutions which are competitive with GW SCS and CVXOPT. For exact solutions, QAOA is also competitive, but with evidence of an exponential dependence on r , especially for Erdős. Results for the classical solvers for these instance sizes should be taken in the context of the asymptotic performance noted in Appendix A.

discuss them in Appendix A. Here we mention that the advantage of heuristic algorithms is more relevant for large N , where its better scaling takes over small size effects and certain details of the implementation. For these system sizes, the approximation ratio achieved by GW is more relevant to the performance comparison.

Figure 6 shows the WallTime performance of the optimized variational parameters from Figure 4 for different graph types and graph sizes up to $N = 32$. Here we take advantage of the recent observation that good parameter values are concentrated and shared among instances of the same type. We empirically verify that good parameter values can be applied to instances with more vertices. By offloading the cost of the parameter optimization, the WallTime performance of QAOA for 3- and 9-regular graphs remains competitive with classical solvers. We observe an exponential increase of the WallTime before reaching approximation ratio close to 1, indicating an exponentially smaller value of $P_{\text{Cut}}(|c^*|)$ compared to, for example, $P_{\text{Cut}}(0.9|c^*|)$. This behavior is very clear for Erdős graphs. For 3- and 9-regular, there is some ev-

idence of linear/sublinear behavior in WallTime versus approximation ratio, another indication of the effective overlap of the distributions shown in Figures 1 and 4 with the maximum cut.

V. DISCUSSION

The results discussed in Sections III and IV demonstrate how much QAOA’s performance depends on the graph type and optimization method. There is a fundamental performance gap between 3- and 9-regular and the Erdos and random weights graph types. The transformation of the optimization landscape (Figure 2 and, indirectly, Figure 3) results in the need for a larger optimization budget ($n_{\text{fev}} > 25,000$) and an inability for the p considered to produce states $|\gamma, \beta\rangle$ with large overlap with the maximum cut for Erdos and random weight graph types. In this context, a very practical question is how to adapt the QAOA protocol to specific graph types and, more generally, to the class of problem instances.

The strong performance dependence on graph type is also true for classical exact and approximate solvers. For example, we observe a correlation between the time required by AKMAXSAT and the vertex degree of the graph. This is confirmed by the trivial case of fully connected graphs, in which any balanced assignment with $N/2$ vertices in both partitions is a global solution: AKMAXSAT requires a time exponential with N and with a much larger exponent than any other graph type.

An intuitive, but central, observation of our study is that, by utilizing the parameters optimized from small instance sizes, the WallTime for large instance sizes is dramatically reduced. The parameters’ optimization can be compared to a training process and its cost off-loaded to a preliminary phase. This is the difference between the blue lines of Figure 5 where no training is assumed, to the orange lines in Figure 5 and Figure 6 where the sampling starts from pre-trained parameters. This additional cost in terms of circuit evaluations is up to $n_{\text{fev}} S = 2.5 \times 10^7$ and, when converted to WallTime, is on the order of 10–100 s. This is the same order of magnitude reported in reference [54].

As a consequence, the WallTime performance reported in Figure 6 depends critically on minimizing the training process by utilizing previously-trained parameters. Our results suggest that the effectiveness of this approach varies significantly for the graph types studied, and more work is necessary to assess how this process scales to instance sizes larger than $N \sim 50$. Along the same lines of avoiding the training phase, recent works propose the use of machine learning techniques [44], [55] or a mix of analytical and numerical results at $N \rightarrow \infty$ [46] to identify good parameters.

Finally, we comment on the choice of the number of QAOA steps. In this work, we have fixed p at the beginning of the optimization. However, there is growing evidence of the need for p increasing with instance size N , without a clear understanding of the exact dependence [28], [40], [41]. From a practical perspective, one may want to extend the optimization process with an adaptive search of p . For the small graphs considered in this study, Figure 4 (b) suggests that such overhead is unjustified when the goal is minimizing QAOA’s WallTime. In fact, the main difference from $p = 2$ to $p = 8$ is the reduced variance of the distribution over instances of the same graph type, without a pronounced reduction of the number of circuit repetitions (also, notice that circuits with $p = 8$ take longer to execute than circuits with $p = 2$).

VI. CONCLUSIONS

We introduced new performance metrics for characterizing the performance of QAOA, focusing on the probability of observing a sample above a certain quality. In this work, given a desired approximation ratio, we formulate the performance of QAOA as the time needed before at least one sample with approximation ratio above the desired threshold is observed with probability at least 50%.

By combining this new approach with “training” of the QAOA variational parameters, our results show a reduction in the QAOA execution time for Max-Cut on random 3-regular graphs of two orders of magnitude with respect to previous estimates [54]. This was possible due to the reduction in number of samples in the calculation of the average approximation ratio, and because we do not wait for the convergence of the parameters’ optimization before analyzing the candidate solutions obtained as single samples.

For other graph types, namely Erdős and random weight, the performance of QAOA varies significantly. While our sampling-based results show remarkable performance improvement for the instance sizes studied, the actual performance test for approximate solution requires its assessment for instance sizes $\sim 100 - 1,000$ depending on the graph type (see Appendix A). To this end, more work is needed to study how effective the training and sampling can be extended to more challenging instance sizes, and how this approach can be extended beyond fixed p (for example a mild dependence $p \propto \log(N)$) while including the effect of noise in the analysis.

ACKNOWLEDGEMENT

This material is based upon work funded and supported by the Department of Defense under Contract

No. FA8702-15-D-0002 with Carnegie Mellon University for the operation of the Software Engineering Institute, a federally funded research and development center. Carnegie Mellon® is registered in the U.S. Patent and Trademark Office by Carnegie Mellon University. DM20-0424

This work used the Extreme Science and Engineering Discovery Environment (XSEDE), which is supported by National Science Foundation grant number ACI-1548562. Specifically, it used the Bridges system, which is supported by NSF award number ACI-1445606, at the Pittsburgh Supercomputing Center (PSC).

REFERENCES

- [1] John Preskill. Quantum Computing in the NISQ era and beyond. *Quantum*, 2:79, August 2018.
- [2] Frank Arute, Kunal Arya, Ryan Babbush, Dave Bacon, Joseph C. Bardin, Rami Barends, Rupak Biswas, Sergio Boixo, Fernando G. S. L. Brandao, David A. Buell, Brian Burkett, Yu Chen, Zijun Chen, Ben Chiaro, Roberto Collins, William Courtney, Andrew Dunsworth, Edward Farhi, Brooks Foxen, Austin Fowler, Craig Gidney, Marissa Giustina, Rob Graff, Keith Guerin, Steve Habegger, Matthew P. Harrigan, Michael J. Hartmann, Alan Ho, Markus Hoffmann, Trent Huang, Travis S. Humble, Sergei V. Isakov, Evan Jeffrey, Zhang Jiang, Dvir Kafri, Kostyantyn Kechedzhi, Julian Kelly, Paul V. Klimov, Sergey Knysh, Alexander Korotkov, Fedor Kostritsa, David Landhuis, Mike Lindmark, Erik Lucero, Dmitry Lyakh, Salvatore Mandrà, Jarrod R. McClean, Matthew McEwen, Anthony Megrant, Xiao Mi, Kristel Michelsen, Massoud Mohseni, Josh Mutus, Ofer Naaman, Matthew Neeley, Charles Neill, Murphy Yuezheng Niu, Eric Ostby, Andre Petukhov, John C. Platt, Chris Quintana, Eleanor G. Rieffel, Pedram Roushan, Nicholas C. Rubin, Daniel Sank, Kevin J. Satzinger, Vadim Smelyanskiy, Kevin J. Sung, Matthew D. Trevithick, Amit Vainsencher, Benjamin Villalonga, Theodore White, Z. Jamie Yao, Ping Yeh, Adam Zalcman, Hartmut Neven, and John M. Martinis. Quantum supremacy using a programmable superconducting processor. *Nature*, pages 1–7, October 2019.
- [3] Sergio Boixo, Sergei V. Isakov, Vadim N. Smelyanskiy, Ryan Babbush, Nan Ding, Zhang Jiang, Michael J. Bremner, John M. Martinis, and Hartmut Neven. Characterizing quantum supremacy in near-term devices. *Nature Physics*, 14(6):595–600, June 2018.
- [4] C. Neill, P. Roushan, K. Kechedzhi, S. Boixo, S. V. Isakov, V. Smelyanskiy, A. Megrant, B. Chiaro, A. Dunsworth, K. Arya, R. Barends, B. Burkett, Y. Chen, Z. Chen, A. Fowler, B. Foxen, M. Giustina, R. Graff, E. Jeffrey, T. Huang, J. Kelly, P. Klimov, E. Lucero, J. Mutus, M. Neeley, C. Quintana, D. Sank, A. Vainsencher, J. Wenner, T. C. White, H. Neven, and J. M. Martinis. A blueprint for demonstrating quantum supremacy with superconducting qubits. *Science*, 360(6385):195–199, April 2018.
- [5] Edward Farhi and Aram W. Harrow. Quantum Supremacy through the Quantum Approximate Optimization Algorithm. *arXiv:1602.07674 [quant-ph]*, October 2019. arXiv: 1602.07674.
- [6] Michael J. Bremner, Ashley Montanaro, and Dan J. Shepherd. Achieving quantum supremacy with sparse and noisy commuting quantum computations. *Quantum*, 1:8, April 2017.
- [7] BAHRAM ALIDAEE, GARY A. KOCHENBERGER, and AHMAD AHMADIAN. 0-1 Quadratic programming approach for optimum solutions of two scheduling problems. *International Journal of Systems Science*, 25(2):401–408, February 1994.
- [8] Hartmut Neven, Geordie Rose, and William G. Macready. Image recognition with an adiabatic quantum computer I. Mapping to quadratic unconstrained binary optimization. *arXiv:0804.4457 [quant-ph]*, April 2008. arXiv: 0804.4457.
- [9] Michel Deza and Monique Laurent. Applications of cut polyhedra — II. *Journal of Computational and Applied Mathematics*, 55(2):217–247, November 1994.
- [10] Manu Jose and Rupak Majumdar. Cause Clue Clauses: Error Localization Using Maximum Satisfiability. In *Proceedings of the 32Nd ACM SIGPLAN Conference on Programming Language Design and Implementation*, PLDI ’11, pages 437–446, New York, NY, USA, 2011. ACM.
- [11] L. Guo, A. S. Vincentelli, and A. Pinto. A complexity metric for concurrent finite state machine based embedded software. In *2013 8th IEEE International Symposium on Industrial Embedded Systems (SIES)*, pages 189–195, June 2013.
- [12] Michael R. Garey and David S. Johnson. *Computers and intractability: a guide to the theory of NP-completeness*. A series of books in the mathematical sciences. Freeman, New York [u.a], 27. print edition, 2009. OCLC: 551912424.
- [13] Edward Farhi, Jeffrey Goldstone, and Sam Gutmann. A Quantum Approximate Optimization Algorithm Applied to a Bounded Occurrence Constraint Problem. *arXiv:1412.6062 [quant-ph]*, December 2014. arXiv: 1412.6062.
- [14] Michel X. Goemans and David P. Williamson. Improved approximation algorithms for maximum cut and satisfiability problems using semidefinite programming. *Journal of the ACM*, 42(6):1115–1145, November 1995.
- [15] Adrian Kügel. Improved Exact Solver for the Weighted Max-SAT Problem. page 38.
- [16] Salvatore Mandrà, Gian Giacomo Guerreschi, and Alán Aspuru-Guzik. Adiabatic quantum optimization in the presence of discrete noise: Reducing the problem dimensionality. *Physical Review A*, 92(6):062320, 2015.
- [17] Salvatore Mandrà, Zheng Zhu, Wenlong Wang, Alejandro Perdomo-Ortiz, and Helmut G. Katzgraber. Strengths and weaknesses of weak-strong cluster problems: A detailed overview of state-of-the-art classical heuristics versus quantum approaches. *Physical Review A*, 94(2):022337, August 2016.
- [18] Iain Dunning, Swati Gupta, and John Silberholz. What Works Best When? A Systematic Evaluation of Heuristics for Max-Cut and QUBO. *INFORMS Journal on Computing*, 30(3):608–624, August 2018.
- [19] Edward Farhi, Jeffrey Goldstone, Sam Gutmann, and Leo Zhou. The Quantum Approximate Optimization Algorithm and the Sherrington-Kirkpatrick Model at Infinite Size. *arXiv:1910.08187 [cond-mat, physics:quant-ph]*, October 2019. arXiv: 1910.08187.
- [20] Andrea Montanari. Optimization of the Sherrington-Kirkpatrick Hamiltonian. *arXiv:1812.10897 [cond-mat]*, April 2019. arXiv: 1812.10897.
- [21] Charles Moussa, Henri Calandra, and Vedran Dunjko. To quantum or not to quantum: towards algorithm selection in near-term quantum optimization. *arXiv:2001.08271 [quant-ph]*, January 2020. arXiv: 2001.08271.
- [22] Edward Farhi, Jeffrey Goldstone, and Sam Gutmann. A quantum approximate optimization algorithm. *arXiv:1411.4028*, 2014.
- [23] Ruslan Shaydulin, Hayato Ushijima-Mesigwa, Ilya Safro, Susan Mniszewski, and Yuri Alexeev. Community Detection Across Emerging Quantum Architectures. *arXiv:1810.07765 [quant-ph]*, October 2018. arXiv: 1810.07765.
- [24] Ruslan Shaydulin and Yuri Alexeev. Evaluating Quantum Approximate Optimization Algorithm: A Case Study. *arXiv:1910.04881 [quant-ph]*, October 2019. arXiv: 1910.04881.
- [25] Gavin E. Crooks. Performance of the Quantum Approximate Optimization Algorithm on the Maximum Cut Problem. *arXiv:1811.08419 [quant-ph]*, November 2018. arXiv: 1811.08419.
- [26] J. S. Otterbach, R. Manenti, N. Alidoust, A. Bestwick, M. Block, B. Bloom, S. Caldwell, N. Didier, E. Schuyler Fried, S. Hong, P. Karalekas, C. B. Osborn, A. Papageorge, E. C. Peterson, G. Prawiroatmodjo, Nick Rubin, C. A. Ryan, D. Scarabelli, M. Scheer, E. A. Sete, P. Sivarajah, R. S. Smith, A. Staley, N. Tezak, W. J. Zeng, A. Hudson, B. R. Johnson, M. Reagor,

M. P. da Silva, and Chad T. Rigetti. Unsupervised machine learning on a hybrid quantum computer. *arXiv:1712.05771*, 2017.

[27] Jeremy Cook, Stephan Eidenbenz, and Andreas Bärtschi. The Quantum Alternating Operator Ansatz on Max-k Vertex Cover. *arXiv:1910.13483 [quant-ph]*, October 2019. arXiv: 1910.13483.

[28] Edward Farhi, David Gamarnik, and Sam Gutmann. The Quantum Approximate Optimization Algorithm Needs to See the Whole Graph: A Typical Case. *arXiv:2004.09002 [quant-ph]*, April 2020. arXiv: 2004.09002.

[29] Pontus Vikstål, Mattias Grönkvist, Marika Svensson, Martin Andersson, Göran Johansson, and Giulia Ferrini. Applying the Quantum Approximate Optimization Algorithm to the Tail Assignment Problem. *arXiv:1912.10499 [quant-ph]*, December 2019. arXiv: 1912.10499.

[30] Abhinav Kandala, Antonio Mezzacapo, Kristan Temme, Maika Takita, Jerry M. Chow, and Jay M. Gambetta. Hardware-efficient variational quantum eigensolver for small molecules and quantum magnets. *Nature*, 549(7671):242–246, 2017.

[31] Guido Pagano, A. Bapat, P. Becker, K. S. Collins, A. De, P. W. Hess, H. B. Kaplan, A. Kyriyanidis, W. L. Tan, C. Baldwin, L. T. Brady, A. Deshpande, F. Liu, S. Jordan, Alexey V. Gorshkov, and Christopher Monroe. Quantum Approximate Optimization with a Trapped-Ion Quantum Simulator. *arXiv:1906.02700*, 2019.

[32] Frank Arute, Kunal Arya, Ryan Babbush, Dave Bacon, Joseph C. Bardin, Rami Barends, Sergio Boixo, Michael Broughton, Bob B. Buckley, David A. Buell, Brian Burkett, Nicholas Bushnell, Yu Chen, Zijun Chen, Ben Chiaro, Roberto Collins, William Courtney, Sean Demura, Andrew Dunsworth, Edward Farhi, Austin Fowler, Brooks Foxen, Craig Gidney, Marissa Giustina, Rob Graff, Steve Habegger, Matthew P. Harrigan, Alan Ho, Sabrina Hong, Trent Huang, L. B. Ioffe, Sergei V. Isakov, Evan Jeffrey, Zhang Jiang, Cody Jones, Dvir Kafri, Kostyantyn Kechedzhi, Julian Kelly, Seon Kim, Paul V. Klimov, Alexander N. Korotkov, Fedor Kostritsa, David Landhuis, Pavel Laptev, Mike Lindmark, Martin Leib, Erik Lucero, Orion Martin, John M. Martinis, Jarrod R. McClean, Matt McEwen, Anthony Megrant, Xiao Mi, Masoud Mohseni, Wojciech Mruczkiewicz, Josh Mutus, Ofer Naaman, Matthew Neeley, Charles Neill, Florian Neukart, Hartmut Neven, Murphy Yuezhen Niu, Thomas E. O’Brien, Bryan O’Gorman, Eric Ostby, Andre Petukhov, Harald Puttermann, Chris Quintana, Pedram Roushan, Nicholas C. Rubin, Daniel Sank, Kevin J. Satzinger, Andrea Skolik, Vadim Smelyanskiy, Doug Strain, Michael Streif, Kevin J. Sung, Marco Szalay, Amit Vainsencher, Theodore White, Z. Jamie Yao, Ping Yeh, Adam Zalcman, and Leo Zhou. Quantum Approximate Optimization of Non-Planar Graph Problems on a Planar Superconducting Processor. *arXiv:2004.04197*, 2020.

[33] Gian Giacomo Guerreschi, Justin Hogaboam, Fabio Baruffa, and Nicolas Per Dane Sawaya. Intel Quantum Simulator: A cloud-ready high-performance simulator of quantum circuits. *Quantum Science and Technology*, 2020.

[34] Intel quantum simulator. <https://github.com/iquisoft/intel-qs>. Accessed: 2020-05-01.

[35] Gian Giacomo Guerreschi. Scheduler of quantum circuits based on dynamical pattern improvement and its application to hardware design. *arXiv:1912.00035*, 2019.

[36] John Adrian Bondy, Uppaluri Siva Ramachandra Murty, and others. *Graph theory with applications*, volume 290. Macmillan London, 1976.

[37] Glen Bigan Mbeng, Rosario Fazio, and Giuseppe E. Santoro. Optimal quantum control with digitized Quantum Annealing. *arXiv:1911.12259*, 2019.

[38] E. Farhi, J. Goldstone, S. Gutmann, and H. Neven. Quantum Algorithms for Fixed Qubit Architectures. *arXiv:1703.06199 [quant-ph]*, March 2017. arXiv: 1703.06199.

[39] M. B. Hastings. Classical and Quantum Bounded Depth Approximation Algorithms. *arXiv:1905.07047 [quant-ph]*, May 2019. arXiv: 1905.07047.

[40] Sergey Bravyi, David Gosset, and Ramis Movassagh. Classical algorithms for quantum mean values. *arXiv:1909.11485 [quant-ph]*, September 2019. arXiv: 1909.11485.

[41] Sergey Bravyi, Alexander Kliesch, Robert Koenig, and Eugene Tang. Obstacles to State Preparation and Variational Optimization from Symmetry Protection. *arXiv:1910.08980 [cond-mat, physics:quant-ph]*, October 2019. arXiv: 1910.08980.

[42] Gian Giacomo Guerreschi and Mikhail Smelyanskiy. Practical optimization for hybrid quantum-classical algorithms. *arXiv:1701.01450 [quant-ph]*, January 2017. arXiv: 1701.01450.

[43] Ruslan Shaydulin, Ilya Safro, and Jeffrey Larson. Multistart Methods for Quantum Approximate Optimization. *arXiv:1905.08768 [quant-ph]*, May 2019. arXiv: 1905.08768.

[44] Sami Khairy, Ruslan Shaydulin, Lukasz Cincio, Yuri Alexeev, and Prasanna Balaprakash. Learning to Optimize Variational Quantum Circuits to Solve Combinatorial Problems. *arXiv:1911.11071 [quant-ph, stat]*, November 2019. arXiv: 1911.11071.

[45] Matteo M. Wauters, Emanuele Panizon, Glen B. Mbeng, and Giuseppe E. Santoro. Reinforcement Learning assisted Quantum Optimization. *arXiv:2004.12323*, 2020.

[46] Michael Streif and Martin Leib. Training the Quantum Approximate Optimization Algorithm without access to a Quantum Processing Unit. *arXiv:1908.08862 [quant-ph]*, August 2019. arXiv: 1908.08862.

[47] Jeffrey Larson and Stefan M. Wild. Asynchronously parallel optimization solver for finding multiple minima. *Mathematical Programming Computation*, 10(3):303–332, September 2018.

[48] M J D Powell. The BOBYQA algorithm for bound constrained optimization without derivatives. page 39.

[49] Leo Zhou, Sheng-Tao Wang, Soonwon Choi, Hannes Pichler, and Mikhail D. Lukin. Quantum Approximate Optimization Algorithm: Performance, Mechanism, and Implementation on Near-Term Devices. *arXiv:1812.01041 [cond-mat, physics:quant-ph]*, December 2018. arXiv: 1812.01041.

[50] Zhihui Wang, Stuart Hadfield, Zhang Jiang, and Eleanor G. Rieffel. Quantum approximate optimization algorithm for MaxCut: A fermionic view. *Physical Review A*, 97(2):022304, February 2018.

[51] Fernando G. S. L. Branda, Michael Broughton, Edward Farhi, Sam Gutmann, and Hartmut Neven. For Fixed Control Parameters the Quantum Approximate Optimization Algorithm’s Objective Function Value Concentrates for Typical Instances. *arXiv:1812.04170 [quant-ph]*, December 2018. arXiv: 1812.04170.

[52] Panagiotis K. Barkoutsos, Giacomo Nannicini, Anton Robert, Ivano Tavernelli, and Stefan Woerner. Improving Variational Quantum Optimization using CVaR. *arXiv:1907.04769 [quant-ph]*, November 2019. arXiv: 1907.04769.

[53] Adrian Kuegel. Improved Exact Solver for the Weighted MAX-SAT Problem. In *EPiC Series in Computing*, volume 8, pages 15–27. EasyChair, May 2012.

[54] G. G. Guerreschi and A. Y. Matsuura. QAOA for Max-Cut requires hundreds of qubits for quantum speed-up. *Scientific Reports*, 9(1):6903, May 2019.

[55] Mahabubul Alam, Abdullah Ash-Saki, and Swaroop Ghosh. Accelerating Quantum Approximate Optimization Algorithm using Machine Learning. *arXiv:2002.01089 [cs]*, April 2020. arXiv: 2002.01089.

[56] Suvrit Sra, Sebastian Nowozin, and Stephen J. Wright. *Optimization for Machine Learning*. MIT Press, September 2011. Google-Books-ID: PNTxCwAAQBAJ.

[57] System configuration.

APPENDIX

A. Classical Performance

The Python CVXOPT library[56] implementation of GW used in this study has large interpreted overhead, making its WallTime performance for very small instance sizes less relevant. Figure 7 confirms that the performance of the exact solver AKMAXSAT[53] is

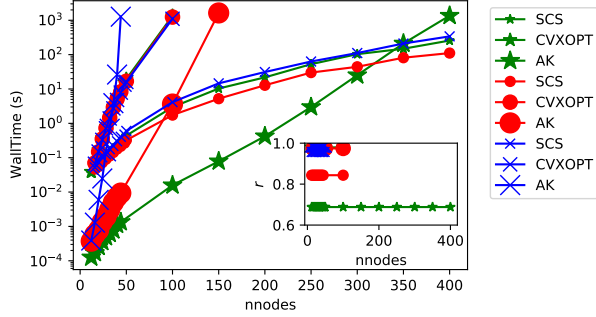


Figure 7: WallTime and approximation ratio performance of classical algorithms AKMAXSAT[53] and the Goemans-Williamson (GW) algorithm[14] for graph types 3-regular (green), 9-regular (red) and Erdős (blue) graph types. For GW, 100 random hyperplanes are used to sample each graph instance, and 10 graph instances are averaged over. These results for nnodes inaccessible by simulation (see Figure 6) demonstrate the asymptotic difference between exact and approximate solver performance (see inset Figure for approximation ratio r).

overtaken by GW at instance sizes that depend on the graph type, but are outside the scope of the simulations of quantum computing discussed in Section III-B. The computational device used to execute these classical solvers is Intel Haswell (E5-2695 v3), utilized in the Pittsburgh Supercomputing Center (PSC) Bridges RM nodes.[57]

B. Random Weight Graphs

Notice that the last graph type has non-unit edge weights. The Max-Cut problem is extended by counting not the number, but the total weight of the edges cut by the partition. In the literature this is known as the weighted Max-Cut problem. In this case, the cut probability p_{cut} is a continuous probability density, and we represent it in discretized form according to $P_{\text{cut}}(c) = \int_c^{c+1} p_{\text{cut}}(c') dc'$.